Noninvasive quantification of metabolic rate of oxygen (MRO2) by photoacoustic microscopy

Junjie Yao, Konstantin I. Maslov, Lihong V. Wang

Junjie Yao, Konstantin I. Maslov, Lihong V. Wang, "Noninvasive quantification of metabolic rate of oxygen (MRO2) by photoacoustic microscopy," Proc. SPIE 7899, Photons Plus Ultrasound: Imaging and Sensing 2011, 78990N (17 February 2011); doi: 10.1117/12.874777

SPIE.

Event: SPIE BiOS, 2011, San Francisco, California, United States

Noninvasive quantification of metabolic rate of oxygen (MRO_2) by photoacoustic microscopy

Junjie Yao, Konstantin I. Maslov, Lihong V. Wang*

Department of Biomedical Engineering, Washington University in St. Louis,

St. Louis, MO 63130, USA

*Corresponding author: lhwang@biomed.wustl.edu

Abstract:

Many diseases, normal decay and physiological functions are closely related to alterations in the metabolic rate of oxygen (MRO_2). In this study, we demonstrate that all the parameters for MRO_2 quantification can be simultaneously obtained by optical-resolution photoacoustic microscopy (OR-PAM). MRO_2 of the mouse ear under normothermia (31 ºC skin temperature) and controlled systematic hyperthermia (42 ºC skin temperature) was studied. As a result of hyperthermia, the MRO_2 increased by 34.1%. The tumor hypermetabolism was also demonstrated by longitudinally monitoring a melanoma growing on a mouse ear. The results show that OR-PAM, as a single noninvasive imaging modality, is well suited for quantitative MRO_2 measurement in microenvironments.

Keywords:

metabolic rate of oxygen (MRO_2), photoacoustic microscopy, systemic hyperthermia, tumor hypermetabolism

Introduction

Aerobic metabolism provides the primary energy demand of human body [1]. The efficiency of oxygen consumption reflects tissue viability and functionality. Many pathological and physiological functions are closely related to alterations of oxygen metabolism: examples include cancer [2, 3], diabetes [4, 5], Alzheimer's disease [6], diabetes [7], burns [8], sleeping [9], and physiologic challenges [10]. Therefore, an accurate measurement of MRO_2 has the potential to provide a powerful tool for diagnosis and therapy of cancer and other diseases as well as for metabolism-related pathophysiological studies.

The metabolic rate of oxygen (MRO_2) is the only parameter that directly reflects the rate of oxygen consumption of tissue. If the region of interest has well-defined feeding and draining vessels, we have [11]

$$\mathrm{MRO}_2 = \varepsilon \times C_{\mathrm{Hb}} \times \left(\mathrm{sO}_{2in} \times A_{in} \times \bar{v}_{in} - \mathrm{sO}_{2out} \times A_{out} \times \bar{v}_{out} \right) / W. \quad (1)$$

Here, subscripts *in* and *out* denote feeding and draining vessels, respectively. ε is the oxygen binding capacity of hemoglobin and is usually taken as a constant (1.36 ml O_2/gram hemoglobin) [1]. C_{Hb} is the total hemoglobin concentration (in grams of hemoglobin/ml blood). sO_2 is the average oxygen saturation (in %). A is the cross-sectional area (in mm^2). $\bar{v}$ is the average blood flow speed (in mm/s). W is the weight of the region of interest (in gram).

We demonstrate that all the parameters for MRO_2 quantification can be simultaneously obtained by functional optical-resolution photoacoustic microscopy (OR-PAM). Specifically, the total hemoglobin concentration and oxygen saturation were measured using two-wavelength excitation [12], blood flow velocity was estimated on the basis of photoacoustic Doppler bandwidth broadening [13, 14], and the vessel cross-section and tissue weight was quantified from the structural PA image.

Materials and methods

Photons Plus Ultrasound: Imaging and Sensing 2011, edited by Alexander A. Oraevsky, Lihong V. Wang,
Proc. of SPIE Vol. 7899, 78990N · © 2011 SPIE · CCC code: 1605-7422/11/$18 · doi: 10.1117/12.874777

The OR-PAM system used in this study is shown in Fig. 1 [12, 15-17]. Briefly, a tunable dye laser (CBR-D, Sirah) pumped by a Nd:YLF laser (INNOSAB, Edgewave, 523 nm) is used as the light source. The laser pulses pass through a 25-µm–diameter pinhole and get focused onto the surface of the mouse ear by a microscope objective lens (Olympus 4×, NA=0.1) with a pulse energy of ~100 nJ. The resulting ultrasonic signals are detected by a spherically focused ultrasonic transducer (V2012-BC, Panametrics-NDT), which is placed confocally with the objective. The detected PA signal is then amplified, digitized, and saved. A volumetric image is generated by recording the time-resolved PA signal (A-line) at each horizontal location of the two-dimensional raster scan. The motion controller provides the trigger signals for laser firing, data acquisition, and motor scanning. A transverse resolution of 5 µm and axial resolution of 15 µm are achieved with an penetration depth of more than 700 µm at 570 nm optical wavelength.

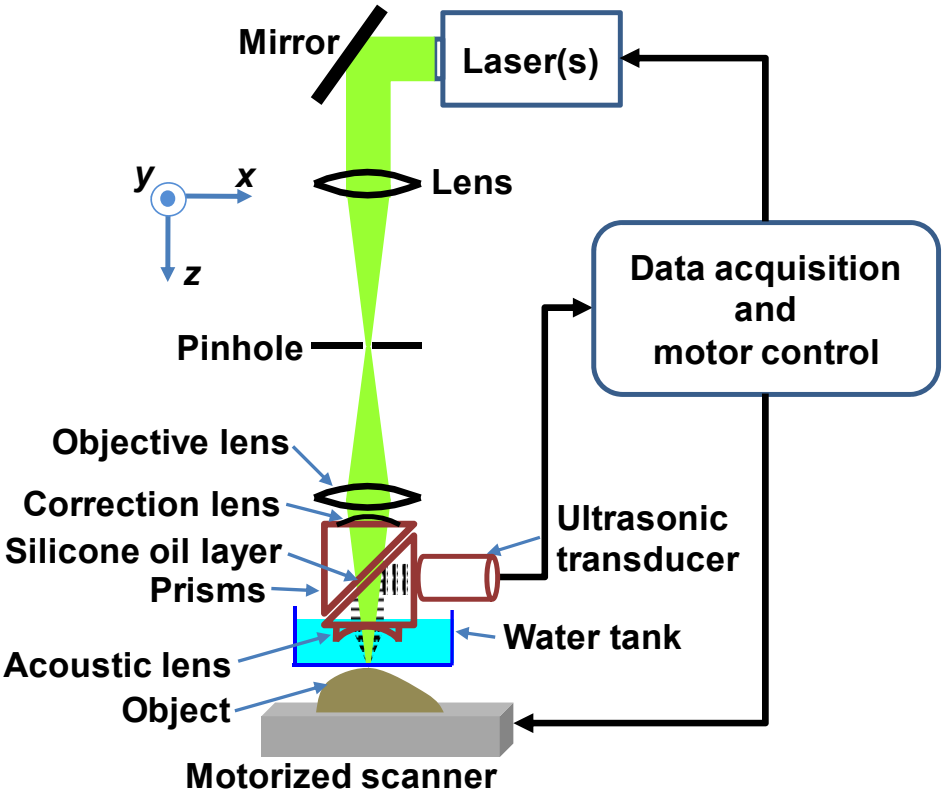

Figure 1. Schematics of optical-resolution photoacoustic microscopy (OR-PAM).

The ears of adult, 6- to 8-week-old nude mice (Hsd: Athymic Nude-Foxl^{NU}, Harlan Co.; body weight: ~20 g) were used for all *in vivo* experiments because of the similarity to human skin and lack of motion artifacts [18-20]. Before data acquisition, the animal was anaesthetized by an intraperitoneal injection of 85% ketamine and 15% xylazine (100 *µl/g* body weight). The animals were kept stable by with a dental/hard palate fixture, and kept still by using a breathing anesthesia system (E-Z Anesthesia, Euthanex). All experimental animal procedures were carried out in conformity with the laboratory animal protocol approved by the Animal Studies Committee of School of Medicine at Washington University in St. Louis.

Results

Change in MRO_2 induced by systemic hyperthermia

Hyperthermia has been found effective in cancer treatment in clinical practice [21-25]. As the first demonstration, we studied MRO_2 of the mouse ear under normothermia (31 ºC skin temperature, shown in Fig. 2) and controlled systemic hyperthermia (42 ºC skin temperature). The experimental results show that hyperthermia increased blood

flow speed [Fig. 3(A)] and vessel diameter. This was caused by the increased heart beating rate and blood redistribution to the skin, which was helpful to accelerate the heat exchange with the environment. We also found that hyperthermia decreased the oxygen extraction fraction (OEF) [Fig. 3(A)]. Because there is a competition in oxygen delivery between oxygen diffusion across the capillary wall and oxygen transport by the blood plasma, increased flow speed shortens the diffusion time and thus decreases OEF [26]. As the net effect, hyperthermia increased the MRO_2 of the mouse ear by 34.1% (n = 3) [Fig. 3(B)]. The increased MRO_2 indicated an elevated oxygen consumption during hyperthermia [21]. These results show that, PAM, as a single noninvasive imaging modality, is intrinsically suitable for quantitative MRO_2 measurement in microenvironments.

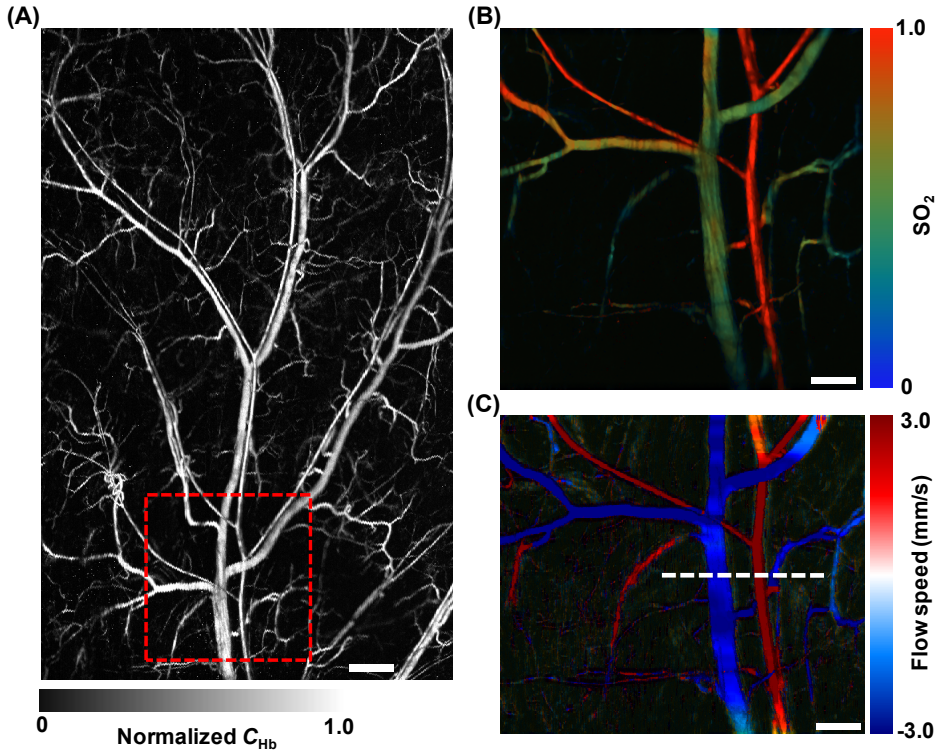

Figure 2. Multi-parametric PAM imaging of mouse ear under normothermia. (A) PAM microvasculature image of a representative mouse ear. Scale bar: 500 µm. (B) Oxygen saturation (sO_2) image of the principal artery-vein pair at the base of the ear [dashed box in (A)]. Scale bar: 250 µm. (C) Blood flow image of the same area of (B). Note the upward flow is defined as positive flow. Scale bar: 250 µm.

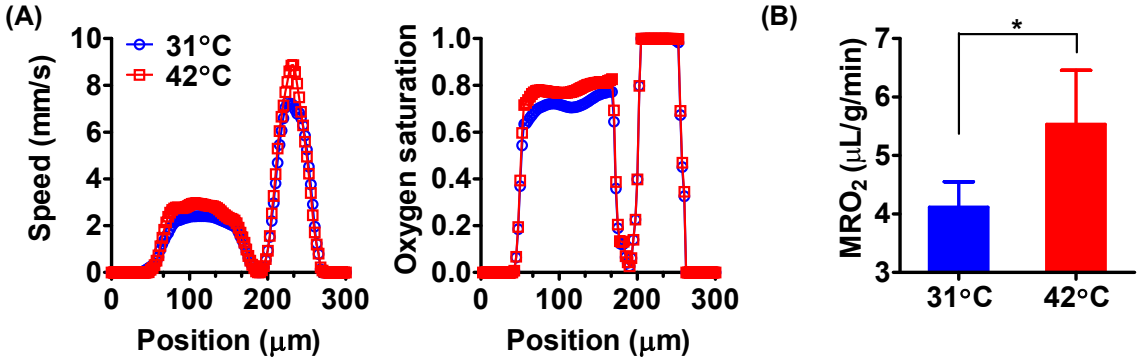

Figure 3. PAM of hemodynamic response to systemic hyperthermia. (A) Profiles of flow speed and oxygen saturation across the principal artery-vein pair under normothermia (31 ºC skin temperature) and controlled systemic hyperthermia (42 ºC skin temperature). (B) Comparison of MRO_2 under normothermia and hyperthermia. Statistics: paired Student's t-test. * $p < 0.05$, $n = 3$.

Change in MRO_2 induced by melanoma growth

As a second demonstration, we longitudinally monitor the MRO_2 of a growing melanoma in a mouse ear. Hemodynamics of the mouse ear after the melanoma cell injection were measured for three weeks. The longitudinally acquired PAM images clearly show vessel dilation around the injection position [Fig. 4(A)], which is critical to meet the increased nutrient demand by the fast tumor growth [27]. From the images acquired at 584 nm and 605 nm, the vasculature and melanoma were differentiated, and the tumor volume was estimated [Fig. 4(A)]. An increase in the oxygen saturation in the supporting vein was observed. This leads to a decrease in the total OEF of the tumor area. Calculated from the above parameters, the total O_2 consumption of the mouse ear increased by 27.3% within 21 days, from 0.11 μl/min to 0.14 μl/min. However, after normalization by the ear weight, we found that the MRO_2 increased by 13.0% from day 0 to day 14, and then decreased by 23.8% from day 14 to day 21. The MRO_2 decline may indicate the necrosis of the tumor core [28], which did not consume oxygen but increase the tissue weight.

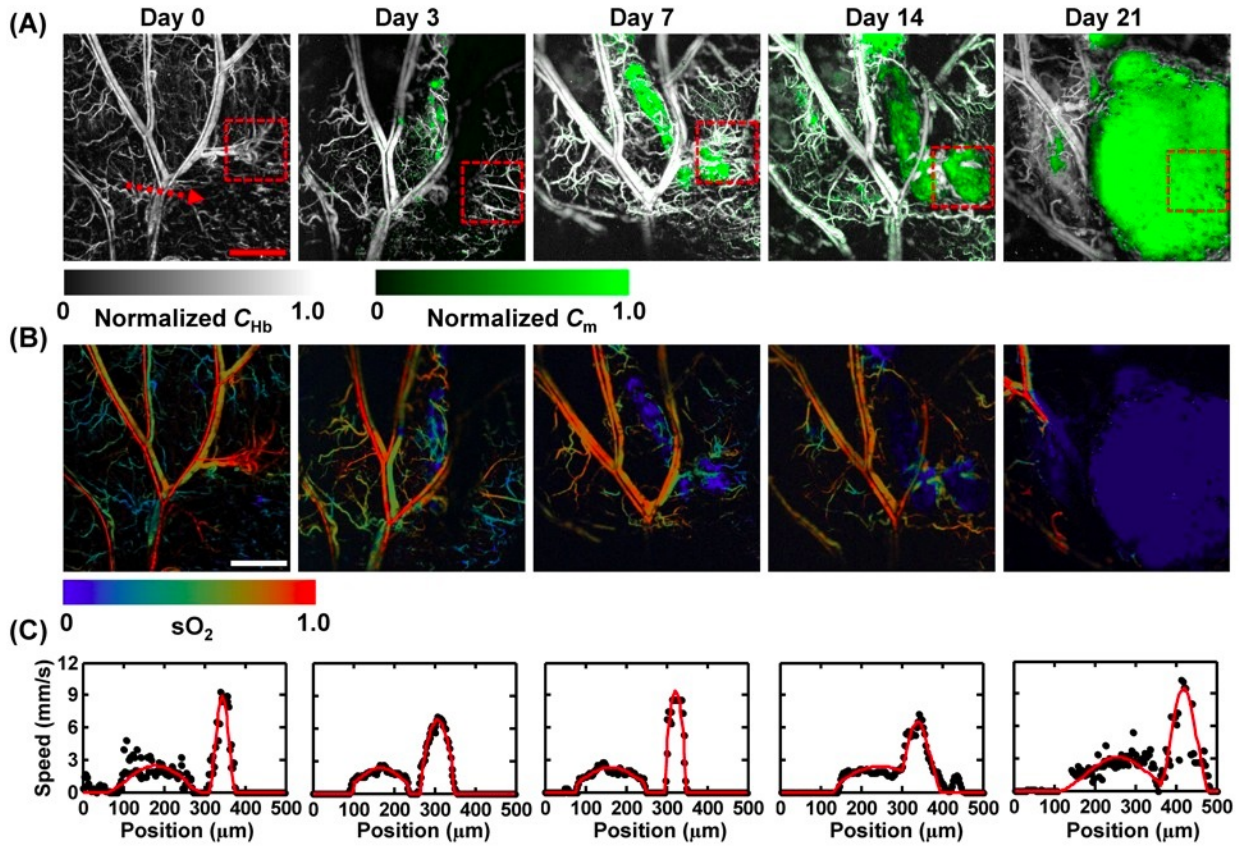

Figure 4. Longitudinal monitoring of melanoma growth. (A) PA vasculature (in gray) and melanoma (in green) imaging from day 0 to day 21. The red dashed boxes are the injection site of tumor cells. Scale bar: 1 mm. C_{Hb}: total hemoglobin concentration; C_m: melanin concentration. (B) Oxygen saturation (sO_2) images. Scale bar: 1 mm. (C) Blood flow profile along the dashed arrow in (A).

Conclusions

In summary, functional optical-resolution photoacoustic microscopy (PAM) is the only imaging modality that is capable of measuring all the parameters that are required for MRO_2 quantification. PAM can potentially be used for various oxygen metabolism associated studies.

Acknowledgements

The authors thank Christopher Favazza, Lidai Wang, Dakang Yao and Arie Krumholz for helpful discussion, Li Li for experimental assistance. This research was supported by the National Institutes of Health Grants R01 EB000712, R01 EB008085, R01 CA134539, U54 CA136398, R01 EB010049, and 5P60 DK02057933. L.V.W. has a financial interest in Microphotoacoustics, Inc. and Endra, Inc., which, however, did not support this work.

References

[1] Guyton, A. C. and Hall, J. E., *Textbook of medical physiology*. 11th ed. 2006, Edinburgh, Oxford: Elsevier Saunders; Elsevier Science distributor. xxxv, 1116 p.

[2] Seyfried, T. N. and Shelton, L. M., "Cancer as a metabolic disease," Nutrition & Metabolism. **7**, 1-22 (2010).

[3] Vaupel, P., Kallinowski, F., and Okunieff, P., "Blood-Flow, Oxygen and Nutrient Supply, and Metabolic Microenvironment of Human-Tumors - a Review," Cancer Research. **49**(23), 6449-6465 (1989).

[4] Stumvoll, M., et al., "Metabolic Effects of Metformin in Non-Insulin-Dependent Diabetes-Mellitus," New England Journal of Medicine. **333**(9), 550-554 (1995).

[5] Karelis, A. D., et al., "Metabolic and body composition factors in subgroups of obesity: What do we know?," Journal of Clinical Endocrinology & Metabolism. **89**(6), 2569-2575 (2004).

[6] Zhang, X. and Le, W. D., "Pathological role of hypoxia in Alzheimer's disease," Experimental Neurology. **223**(2), 299-303 (2010).

[7] Cheng, K., et al., "Hypoxia-inducible factor-1 alpha regulates beta cell function in mouse and human islets," Journal of Clinical Investigation. **120**(6), 2171-2183 (2010).

[8] Tadros, T., Traber, D. L., and Herndon, D. N., "Hepatic blood flow and oxygen consumption after burn and sepsis," Journal of Trauma-Injury Infection and Critical Care. **49**(1), 101-108 (2000).

[9] Maquet, P., "Sleep Function(S) and Cerebral Metabolism," Behavioural Brain Research. **69**(1-2), 75-83 (1995).

[10] Lin, A. L., et al., "Nonlinear coupling between cerebral blood flow, oxygen consumption, and ATP production in human visual cortex," Proceedings of the National Academy of Sciences of the United States of America. **107**(18), 8446-8451 (2010).

[11] Wang, L. V., "Prospects of photoacoustic tomography," Medical Physics. **35**(12), 5758-5767 (2008).

[12] Hu, S., Maslov, K., and Wang, L. H. V., "In vivo functional chronic imaging of a small animal model using optical-resolution photoacoustic microscopy," Medical Physics. **36**(6), 2320-2323 (2009).

[13] Yao, J., et al., "In vivo photoacoustic imaging of transverse blood flow by using Doppler broadening of bandwidth," Opt. Lett. **35**(9), 1419-1421 (2010).

[14] Yao, J. and Wang, L. V., "Transverse flow imaging based on photoacoustic Doppler bandwidth broadening," Journal of Biomedical Optics. **15**(2), 021304 (2010).

[15] Hu, S., et al., "Functional transcranial brain imaging by optical-resolution photoacoustic microscopy," Journal of Biomedical Optics. **14**(4), 040503 (2009).

[16] Hu, S., Maslov, K., and Wang, L. H. V., "Noninvasive label-free imaging of microhemodynamics by optical-resolution photoacoustic microscopy," Optics Express. **17**(9), 7688-7693 (2009).

[17] Hu, S. and Wang, L. V., "Photoacoustic imaging and characterization of the microvasculature," Journal of Biomedical Optics. **15**(1), 011101 (2010).

[18] Eriksson, E., Boykin, J. V., and Pittman, R. N., "Method for in vivo microscopy of the cutaneous microcirculation of the hairless mouse ear," Microvascular Research. **19**(3), 374-379 (1980).

[19] Barker, J. H., et al., "The Hairless Mouse Ear for in Vivo Studies of Skin Microcirculation," Plastic and Reconstructive Surgery. **83**(6), 948-959 (1989).

[20] Rins, M., et al., "Skin density in the hairless rat. Evidence of regional differences," Eur J Drug Metab Pharmacokinet. **Spec No 3**, 456-7 (1991).

[21] Dudar, T. E. and Jain, R. K., "Differential Response of Normal and Tumor Microcirculation to Hyperthermia," Cancer Research. **44**(2), 605-612 (1984).

[22] Hahn, G. M., "Metabolic Aspects of Role of Hyperthermia in Mammalian-Cell Inactivation and Their Possible Relevance to Cancer Treatment," Cancer Research. **34**(11), 3117-3123 (1974).
[23] Ito, A., et al., "Tumor regression by combined immunotherapy and hyperthermia using magnetic nanoparticles in an experimental subcutaneous murine melanoma," Cancer Science. **94**(3), 308-313 (2003).
[24] Pettigre.Rt, et al., "Circulatory and Biochemical Effects of Whole-Body Hyperthermia," British Journal of Surgery. **61**(9), 727-730 (1974).
[25] Rhind, S. G., et al., "Contribution of exertional hyperthermia to sympathoadrenal-mediated lymphocyte subset redistribution," Journal of Applied Physiology. **87**(3), 1178-1185 (1999).
[26] Buxton, R. B. and Frank, L. R., "A model for the coupling between cerebral blood flow and oxygen metabolism during neural stimulation," Journal of Cerebral Blood Flow and Metabolism. **17**(1), 64-72 (1997).
[27] Mahabeleshwar, G. H. and Byzova, T. V., "Angiogenesis in melanoma," Semin Oncol. **34**(6), 555-65 (2007).
[28] Sutherland, R. M., "Cell and Environment Interactions in Tumor Microregions - the Multicell Spheroid Model," Science. **240**(4849), 177-184 (1988).